Unlocking the potential of bio-inspired bioinks: A collective breakthrough in mammalian tissue bioprinting

Christophe Marquette, Laura Chastagnier, Benjamin da Sousa, Carlos Chocarro-Wrona, Edwin-Joffrey Courtial, Elea Rae, Céline Thomann, Albane Carre, Lucie Essayan, Ana Pasuch, et al.

▶ **To cite this version:**

Christophe Marquette, Laura Chastagnier, Benjamin da Sousa, Carlos Chocarro-Wrona, Edwin-Joffrey Courtial, et al.. Unlocking the potential of bio-inspired bioinks: A collective breakthrough in mammalian tissue bioprinting. Bioprinting , 2024, 41, pp.e00351. 10.1016/j.bprint.2024.e00351 . hal-04729007

HAL Id: hal-04729007
https://hal.science/hal-04729007v1

Submitted on 9 Oct 2024

HAL is a multi-disciplinary open access archive for the deposit and dissemination of scientific research documents, whether they are published or not. The documents may come from teaching and research institutions in France or abroad, or from public or private research centers.

L'archive ouverte pluridisciplinaire **HAL**, est destinée au dépôt et à la diffusion de documents scientifiques de niveau recherche, publiés ou non, émanant des établissements d'enseignement et de recherche français ou étrangers, des laboratoires publics ou privés.

Bioprinting 41 (2024) e00351

Contents lists available at ScienceDirect

Bioprinting

journal homepage: www.sciencedirect.com/journal/bioprinting

Unlocking the potential of bio-inspired bioinks: A collective breakthrough in mammalian tissue bioprinting

Christophe A. Marquette [a,*], Laura Chastagnier [a], Benjamin Da Sousa [a], Carlos Chocarro-Wrona [a], Edwin-Joffrey Courtial [a], Elea Rae [a], Céline Thomann [a], Albane Carre [a], Lucie Essayan [a], Ana J. Pasuch [a], Alizée Mosnier [a], Chloé Devillard [a], Emma Petiot [a], Lucas Lemarié [b], Eva-Laure Matera [c], Meigge Simoes [c], Charles Dumontet [c], Cristina Cuella Martin [d], Léa Pechtimaldjian [d], Eve-Isabelle Pécheur [d], Véronique Maguer-Satta [d], Maude Michelet [e], Marie-Laure Plissonnier [e], Fabienne Archer [f], Karen Moreau [g], Marjorie Dufaud [h], Cécile Zaupa [i], Jean-Marc Balloul [i], Quentin Pruvost [j], Thibaud Dauphin [j], Mathilde Mosser [j], Sarah Pragnère [k]

[a] 3d.FAB, CNRS, INSA, CPE-Lyon, UMR5246, ICBMS, Universite Claude Bernard Lyon 1, Villeurbanne, Cedex, France
[b] SEGULA Technologies, Bron, France
[c] Oncopharmacologie, Centre de Recherche en Cancérologie de Lyon (CRCL) - UMR INSERM U1052 CNRS 5286 - HCL, 69008, Lyon, France
[d] CITI, Centre de Recherche en Cancérologie de Lyon (CRCL) - UMR INSERM U1052 CNRS 5286 - Centre Léon Bérard, 28 Rue Laënnec, 69008, Lyon, France
[e] Hepatitis Viruses and Pathobiology of Chronic Liver Disease, Centre de Recherche en Cancérologie de Lyon (CRCL) - UMR INSERM U1052 CNRS 5286, 151 Cours Albert Thomas, 69424, Lyon, Cedex 03, France
[f] IVPC UMR754, INRAE, Universite Claude Bernard Lyon 1, EPHE, Lyon, F-69007, Lyon, France
[g] CIRI, Centre International de Recherche en Infectiologie, Inserm U1111, Universite Claude Bernard Lyon 1, CNRS UMR5308, ENS de Lyon, Lyon, France
[h] IRMB, 80 Av. Augustin Fliche, 34000, Montpellier, France
[i] Transgene, 400 Boulevard Gonthier d'Andernach, Parc d'Innovation – CS80166, 67405, Illkirch-Graffenstaden, France
[j] ONIRIS VetAgroBio Nantes, INRAE, Immuno-Endocrinologie Cellulaire et Moléculaire (IECM), USC 1383, 101 route de Gachet, 44300, Nantes, France
[k] Laboratory of Tribology and System Dynamics UMR-CNRS 5513, Ecole Centrale de Lyon, France

ARTICLE INFO

Keywords:
Bioink
Bioprinting
Formulation
Human tissues
Hydrogel
Mechanical properties

ABSTRACT

The composition of soft tissues in mammals can be simplified as approximately 60–65 % water, 16 % protein, 16 % fat, 1 % carbohydrate, and trillions of cells. This report brings together unpublished results from a collaborative efforts of 10 research groups over the past five years, all dedicated to producing mammalian tissues through extrusion-based bioprinting. What unified these studies was a common approach, with a shared bioink composition consisting of gelatin, alginate, and fibrinogen, and a post-printing consolidation strategy involving transglutaminase crosslinking, calcium chelation, and thrombin-mediated fibrin production. The range of Young's moduli achievable was 0.17–105 kPa, perfectly align with of tissue properties.

By consolidating the findings of these studies, it was conclusively demonstrated that bioprinting and culturing all 19 cells tested from 14 different organs was indeed achievable. These remarkable outcomes were attributed not only to the bio-inspired nature of the common bioink but also to its unique rheological properties, such as significant shear-thinning and a sufficiently high static yield stress.

The majority of these cells exhibited behaviours consistent with their natural *in vivo* environments. Clearly identifiable microstructures and organizations showcased intricate morphogenesis mechanisms resulting in the formation of micro-tubules, micro-vessels, and micro-acini. It is now evident that microextrusion bioprinting, especially when using bio-inspired bioink formulations, represents a promising avenue for generating a wide range of mammalian soft tissues.

* Corresponding author.
E-mail address: christophe.marquette@univ-lyon1.fr (C.A. Marquette).

https://doi.org/10.1016/j.bprint.2024.e00351
Received 7 March 2024; Received in revised form 12 June 2024; Accepted 1 July 2024
Available online 2 July 2024
2405-8866/© 2024 The Authors. Published by Elsevier B.V. This is an open access article under the CC BY license (http://creativecommons.org/licenses/by/4.0/).

1. Introduction

To construct an adult human body, a typical composition includes approximately 60–65 % water, 16 % protein (comprising collagen and other extracellular matrix components), 16 % fat, 1 % carbohydrate, and a multitude of cells [1]. This composition serves as the baseline (except the fat content) when attempting to replicate living soft tissues. In this endeavor, hydrogels have emerged as the most suitable materials [2], particularly when they are crafted from biomolecules like extracellular matrix supramolecular assemblies. In the context of 3D bioprinting, a bio-inspired bioink shall be considered as a hydrogel mimicking as much as possible the soft tissue composition mentioned earlier, in order to implement niches for tissue development.

Abbreviations

AD-MSC	Adipose derived Mesenchymal Stem/Stromal Cell
CAF	Cancer Associated Fibroblasts
CHO	Chinese Hamster Ovary
DMA	Dynamic Mechanical Analysis
DMEM	Dulbecco's modified eagle's medium
ECM	ExtraCellular Matrix
HOB	Human Osteoblast
HMEC-1	Human Microvascular Endothelial Cell
HUVEC	Human Umbilical Vein Cell
MDCK	Madin-Darby Canine Kidney
NHLF	Normal Human Lung Fibroblast

In the field of tissue engineering, these assemblies primarily revolve around collagen (sourced from animals or plants [3]) and polysaccharides (such as alginate from algae, gellan gum from bacteria, and chitosan from arthropods or crustaceans [4]), often supplemented with various specific molecules like fibrinogen, fibronectin, hyaluronic acid, methyl cellulose, and decellularized extracellular matrix components [5].

In addition to their composition, soft tissues are distinguished by their mechanical properties, primarily characterized by their Young's modulus, which varies from 1 kPa for brain tissue to 1 MPa for cartilage [6]. Achieving the appropriate mechanical properties is essential and must align with the previously mentioned composition. Furthermore, the specific and intricate shapes of tissues and organs are integral to their functions, provided that the cellular makeup is accurately replicated. Currently, microextrusion-based 3D bioprinting of hydrogel is the only method capable of producing these complex shapes [7]. Of course other 3D bioprinting methods (droplet based; laser assisted; volumetric) are complementary, but the scaling-up of the methods is still only relying on extrusion.

The ongoing pursuit of tissue engineers is to construct 3D living structures that closely mimic the composition and mechanical properties of *in vivo* conditions. Over the last five years, 10 research groups have collectively dedicated ourselves to this pursuit, commencing with the development of a 3D printable hydrogel formulation [8] compatible with the bioprinting of sizable living tissues [9]. This formulation combines alginate, gelatin, and fibrinogen, and it is consolidated in the presence of thrombin, calcium, and transglutaminase (as shown in Fig. 1). The initial cells introduced into this hydrogel were fibroblasts from the human dermis, which exhibited growth and migration throughout the entire 3D construct while producing newly synthesized extracellular matrix. We have even succeeded in validating a medical-grade version of this bioink suitable for direct clinical applications [10].

In this report, we demonstrate how this initial formulation, along with its reticulation conditions, can be finely adjusted to create cellularized hydrogels with a broad range of mechanical properties while maintaining cell proliferation. This extensive study involved over 19 mammalian cell types sourced from both healthy and pathological tissues, including cell aggregates such as human pancreatic pseudo-islets.

2. Results

2.1. Printability: shear thinning and static yield stress

The bio-inspired bioink was designed for microextrusion-based bioprinting. In this bioprinting process, cell laden hydrogels are extruded through a nozzle of known diameter (100–800 µm) and geometry (tronconical or linear) [11]. As a consequence of the viscous bioink travelling through the nozzle, shear forces are inevitably generated upon cells during the extrusion process [12]. We have previously shown [13] that the cell survival was impaired by shear stress affecting membrane integrity, leading to cell lysis, and to a lower extent to cell necrosis and apoptosis [14]. The magnitude of these forces depends on temperature [15], nozzle geometry but also on the flow rate applied to perform the extrusion [16]. When all these parameters are constant, the cell viability

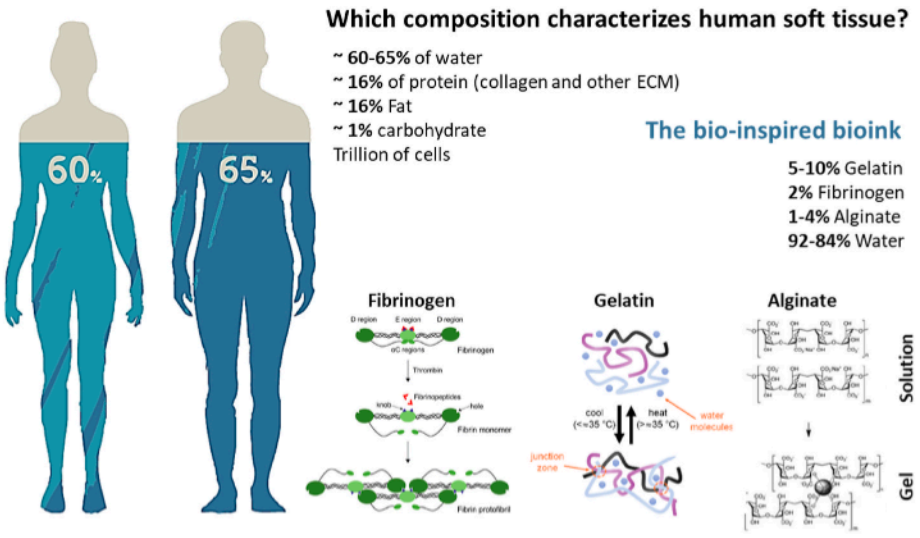

Fig. 1. Concept and composition of the bio-inspired bioink. The bioink recapitulates the mean human body composition using three well defined macromolecular assemblies. Presentation of the 3 components of the bioink together with their consolidation mechanisms.

is finally driven by the bioink shear thinning behaviour [17].

When planning to 3D bioprint large complex living structures, another paramount rheological behaviour is the static yield stress value (τ_y^s) of the material at the printing temperature. Studies have already linked this static yield stress to the material's printability when using microextrusion technique [18]: the higher the yield stress value, the more complex the 3D printed structures can be [19].

Within the 10 bioink formulations described in this study, the rheological behaviours of 7 of them (BI-1 to −7) were studied in detail. These formulations were chosen for their representativeness of the full range of formulation possibilities. The common approach to evaluate alginate/gelatin bioink rheology is the critical shear rate experiment which enables the identification of the important shear thinning behaviour mentioned above. Examples of these measurements for 3 formulations (BI-1, 5 and 6) are presented in Fig. 2-A. As expected, the viscoelastic behaviour of the bioinks evidenced a decrease of viscosity with increasing shear, typical of a shear-thinning behaviour.

To go deeper in the understanding of the 7 bioinks' rheological behaviour, dynamic analyses of phase angle at rest and at flow were characterised (Fig. 2-B). These dynamic analyses unveiled the evolution of the viscoelastic balance of the 7 bioinks before and after shear rate (10 s^{-1} during 30 s). This approach enabled us to demonstrate two important effects of varying the gelatin proportion (w/total w) within the bioinks. First, when this proportion was higher than 3, the phase angles at flow and at rest were similar. On the contrary, when this proportion was lower than 3, these phase angles started to deviate from each other, suggesting a plastic effect. Second, increasing the gelatin proportion from 0 to 7.5 induced a reduction of both angles, demonstrating a clear gain in elasticity. This behaviour was expected since gelatin is a macromolecular network, already shown in previous studies to play a major role in hydrogels' elasticity [20]. Another interesting information here is that we found a direct and linear relationship between the gelatin proportions (wt./other components wt.) within the bioinks and the bioink storage modulus G' value (Fig. 2-C).

Similarly, when looking at the impact of increasing the gelatin proportion upon the static yield stress values, an interesting behaviour was identified (Fig. 2-D). Indeed, before shearing, increasing the gelatin proportion led to increased static yield stress, but after shearing, gelatin proportions higher than 1.25 led to a constant mean 650 Pa static yield stress. It was then clear that the applied shear ($30s^{-1}$, equivalent to the shear generated during bioprinting using a 410 µm diameter nozzle and a flow rate of 5 µL/s) [13] broke the bioink microstructures and led to a capped static yield stress.

In conclusion, from a bioprinting stand point, multiple bio-inspired bioink formulations were able to fulfil the printability requirements. They are all shear-thinning, and except for the BI-5, they all present a high enough static yield stress [19]. It is possible to envision the tuning of the formulation to reach multiple final properties like Young's modulus, without hindering printability.

Out of the studied 7 formulations, BI-1 has a special position since it is the one giving the best static yield stress value, with the lowest gelatin proportion, but also a moderate plastic effect and a marked shear-thinning behaviour. For all these reasons, BI-1 was the most commonly used bioink in the following studies.

2.2. Range of reachable mechanical properties: DMA measurements

Being able to tune the mechanical properties of a hydrogel is a must when trying to recapitulate multiple tissues or organs. Indeed, each soft tissue is characterised by its mechanical property (mainly described by its Young's modulus). This is of course a simplified view of the reality, and each tissue or organ is a composite of different Young's moduli. Nevertheless, these moduli for soft tissues range from 1 kPa for the brain to 1 MPa for the cartilage [6]. In the present approach, we have investigated the range of achievable Young's moduli using only 3 components (i.e. gelatin, alginate and fibrinogen) and 3 gelation reactions (i.e.

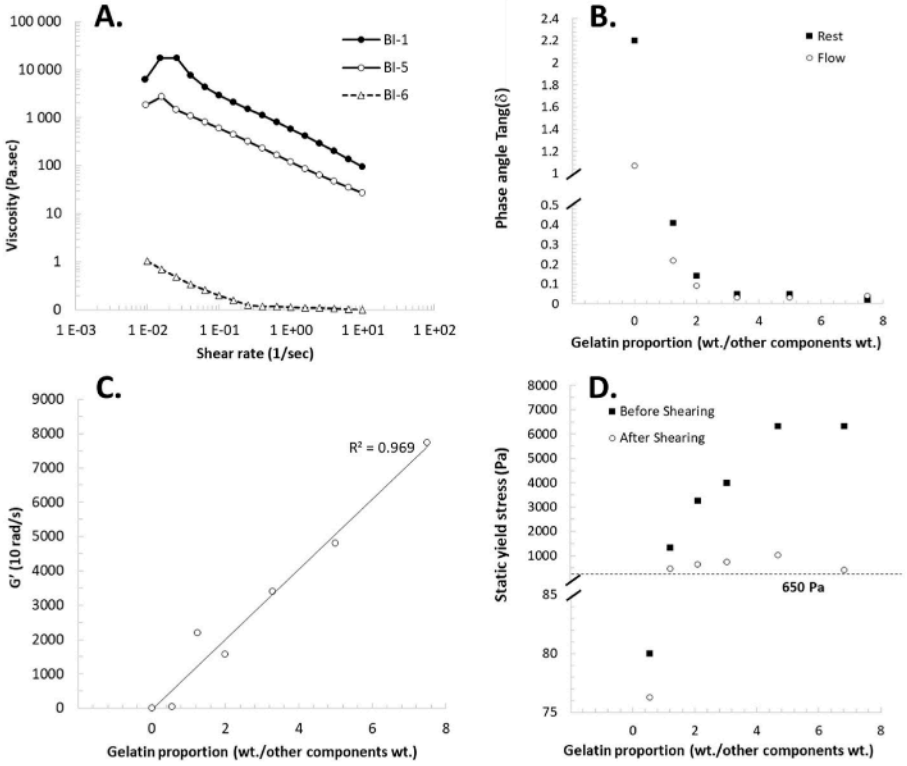

Fig. 2. Rheological characterisations of the bio-inspired bioink. A) Critical shear rate determination of BI-1, BI-5 and BI-6. B/Phase angle evolution, at rest and at flow, according to the gelatin proportion (wt./other components wt.). C) G′ evolution according to gelatin proportion in the bioink. D) Evolution of the static yield stress, before and after shearing at $30s^{-1}$, according to the gelatin proportion in the final bioink. All measurements were performed at 21 °C.

transglutaminase crosslinking, calcium chelation and thrombin mediated fibrin production, Fig. 1). Fig. 3-A presents the concatenation of all the 32 conditions tested, depicting their respective Young's moduli. The full data set can be found as Supplementary Table S2. As can be seen, playing with both the 12 bioink formulations and the 24 consolidation conditions, enabled us to cover the 0.17–105 kPa range. In an attempt to extract more information from these data, Fig. 3-B representation has been built to highlight the calcium and transglutaminase collaborative effect. We chose to focus on the BI-1 composition as it is the one for which the largest collection of data was available. A clear increase of Young's moduli was found as a function of both transglutaminase and calcium concentration in the consolidation solution. This observation was expected since both consolidation reactions are generating cross-linking nodes within the supramolecular assembly. Moreover, the transglutaminase being a calcium-dependent enzyme [21], the presence of calcium most likely has a dual effect: increasing the alginate network crosslinking as well as activating the transglutaminase activity.

Interestingly, using one single bio-inspired bioink formulation (BI-1) was sufficient to cover Young's moduli values ranging from 170 Pa to 46.7 kPa.

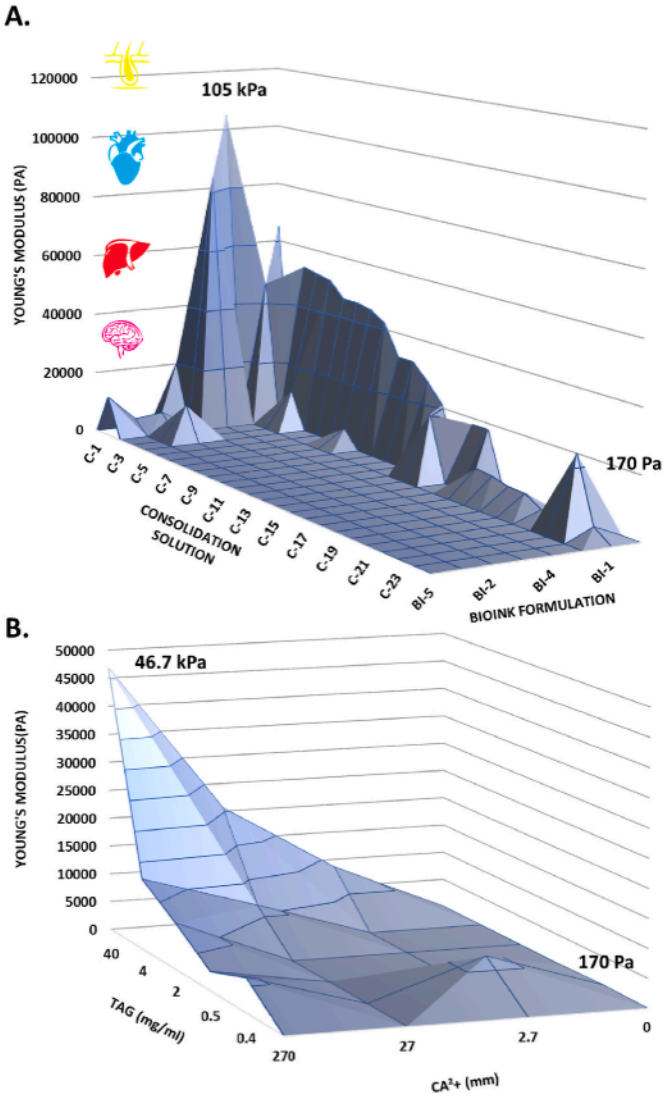

Fig. 3. Mechanical modulation of the bio-inspired bioink. A) Young's modulus as a function of the consolidation solution and the bioink formulation. B) Collaborative effect of the calcium and transglutaminase concentration on the Young's modulus of the BI-1 bioink.

2.3. Cell development and tissue organisation

Once printability established and mechanical properties characterised, the next step in the development of a bio-inspired bioink for tissues and organs production shall be its ability to host and grow the largest variety of mammalian cells (human and animal). For the last 5 years, we have been studying the development of 19 different cell types, coming from 10 different tissues (See Supplementary Table S1). For each cell type and tissue, consolidation conditions were optimized by each research group according to cell growth but also tissue development. Also, seeding density was empirically optimized for each cell type according to their growth capacity and the quality of the obtained final tissue. It is worth to mention that cell homeostasis within the hydrogel was essential to generate stable tissue and that this homeostasis is highly impacted by the number and type of cells.

In order to standardise this large set of results, lactate production was used as an indicator of the cellular development within the bio-inspired bioink. This analytical parameter not only reflects the number of cells but also their metabolic status. In the present report, we made the assumption that the preferential metabolic pathway of the different cell types did not significantly change during the monitored 3D culture time (between 15 and 43 days depending on the cell type). The cell development was then expressed as "relative cell population", directly proportional to the lactate content of the culture medium. This assumption implies that depending on the metabolic activity of each particular cell type, the correlation between the increase of measured lactate and the cell number will be different for each cell type. This is why the "relative cell population" was normalised against their final value (last time point collected).

Fig. 4 presents the typical growth profiles of 19 different cell types (0.3 cm^3 objects: 1 cm*1 cm*3 mm) bioprinted using the BI-1 formulation and various consolidation solutions (see Supplementary Table S1) of the bio-inspired bioink. Some tissues were composed of only one cell type while others, such as endothelialized, epithelialized and colorectal tumour ones, were co-cultures with cells of the connective tissue.

A first observation is the versatility in terms of proliferative properties of the bio-inspired bioink that leads to the growth (lactate production increase) of all investigated cell types. However, differences in the apparent growth rate could be seen. Some cell types (NHLF, HUVEC + CAF) present a fast growing profile followed by a plateau, while others (BT-474, SK-BR-3, HOB, AD-MSC, kidney epithelial) grow continuously for more than 25 days, or with multiple growth (or metabolic) phases (fibroblasts, HT29). These differences are to be expected since these cells, coming from various organs, are characterised *in vivo* by rapid or small doubling time [22]), by tissue remodelling capacity or even by self-organisation in functional microstructures (acini, tubules, capillaries …).

Figs. 5–8 presents examples of these cellular organisation and distribution within the bio-inspired bioink. As visible in all cases, cells displayed a 3D organisation, when distributing within the bioink. Moreover, a closer look at the different images enabled the identification of multiple self-organised structures. Endothelial cells (HUVEC) produced microvascular networks in the presence of fibroblasts (Fig. 5-A). Cells of human colon (HT29 (Fig. 6-A) and breast (BT474 (Fig. 6-B)) cancers organised as spheroids populating the entire bioink. At 35 days post printing, HT29 cell clusters are composed of different areas with proliferating cells (Ki67 labelling) at the outer layer and an apoptotic site at the centre (cleaved caspase 3 labelling) of the cell cluster. This heterogeneous composition, typical of tumour organisation, was proved to be correlated with hypoxia through labeling against added pimonidazole (data not shown). Interestingly, kidney immortalised cells (HEK (Fig. 7-C)) were also organized as discrete spheroids within the bioink. This HEK behaviour has already been shown in 3D cultures within similar hydrogels [23].

Cells such as keratinocytes (Fig. 7-B), kidney (VERO (Fig. 8-A)) and lung (Calu-3 (Fig. 7-A)) epithelial cells developed at the surface of the

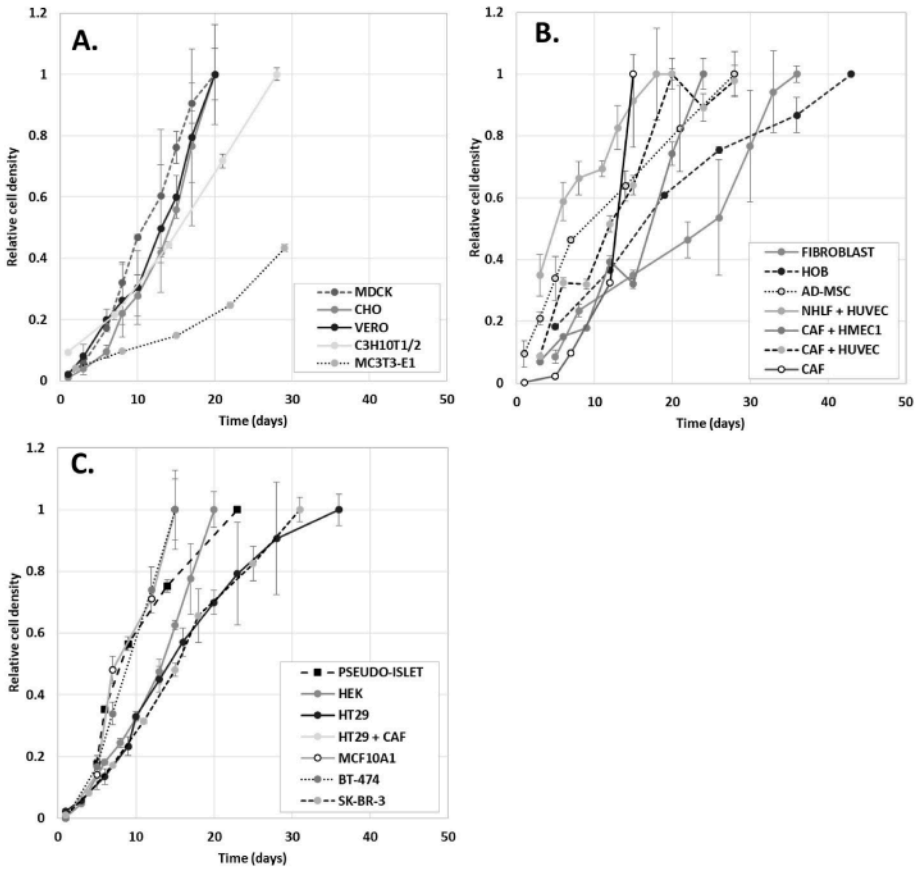

Fig. 4. Typical growth profiles of the 19 different cells (0.3 cm^3 objects: 1 cm*1 cm*3 mm) bioprinted using the BI-1 formulation of the bio-inspired bioink. Relative cell populations are calculated using the cumulated lactate content within the culture medium of each tissue. Curves are normalised according to the maximum signal. N = 2–3. A) Animal cell lines. B) Human primary cells. C) Human cell lines.

bioink, forming typical epithelia layers. On the contrary, the epithelial MDCK cell line (Fig. 8-D), isolated from tubules of a dog's kidney [24], was characterised by the appearance of cellular structures forming a circular cell monolayer defining a lumen, typical of cyst formation. This characteristic structure of kidney tubules was already reported for MDCK cultures in type-I Collagen and Matrigel 3D hydrogels [25]. In a similar way, cells of the human MCF10A (Fig. 6-C) immortalised cell line, a mixture of epithelial, stem and progenitors cells originating from a fibrocystic breast disease, developed and sprouted within the bio-inspired bioink, forming primary and secondary ducts, as already observed in collagen-based hydrogels [26]. CHO cells (Fig. 8-B), originating from fibroblastic cells of the ovary of a Chinese hamster [27], organised as large irregular aggregates, presenting strong similarities with the organisation of the ovary interstitial tissue [28]. Cells of the human HepaRG cell line (Fig. 5-B), differentiated toward the hepatocyte lineage, spread within the bioink, producing typical hepatic markers such as albumin and cytokeratin 18 (CK18) [29]. Human bone cells (HOB (Fig. 5-C)) formed elongated structures, interconnected through their dendrites' network, typical of fully differentiated osteocytes[26]. Human primary adipose tissue-derived mesenchymal stem cells (AD-MSC (Fig. 7-E)) populated the entire bioink, while keeping their original shape [30].

Mouse embryogenic sarcoma stromal cells [31], used to generate cartilage models within the bioink were shown to express high viability at D28, but also chondrocyte cell aggregation [32] in differentiation conditions (Fig. 8-D).

Finally, already formed human Langerhans pseudo-islets (Fig. 7-D) were easily identified within the bioink [33], as they populated the entire volume, as a proof-of-concept that 200–400 µm cell aggregates could be bioprinted using the bio-inspired bioink and maintain their organisation [34]. In this particular case, we noticed that after 5 days of culture, cells escaped the aggregates and spread within the surrounding hydrogel (see insert).

3. Conclusion

The present report consolidates the research efforts of 10 research groups who, over the last five years, have been striving to create mammalian tissues through extrusion-based bioprinting technology. What unites these studies is a shared approach, featuring a common bioink composition and post-printing consolidation strategy.

By compiling the findings of these experiments, we have shown that it is indeed possible to develop bio-inspired bioinks that closely emulate the composition of mammalian soft tissues in terms of protein, carbohydrate, and water content. Additionally, these bioinks exhibit rheological behaviours well-suited for 3D bioprinting, including a desirable shear-thinning quality and a sufficiently high static yield stress. The proportion of gelatin within the bioink can be adjusted to fine-tune these properties. Among the formulations utilizing the three selected components (gelatin, alginate, and fibrinogen), the BI-1 bioink has garnered particular favour among our collaborators due to its printability at 21 °C, without the need for temperature control of the cartridge or building plate. It displays pronounced shear-thinning behaviour and a high static yield stress, facilitating the 3D bioprinting of substantial living constructs [9].

Furthermore, the compilation of these results has shown that a broad spectrum of mechanical properties can be achieved simply by altering the consolidation conditions of the bioink. This adaptability has been widely utilized by our collaborators to adjust the final Young's modulus of their 3D bioprinted constructs to meet the specific requirements of the

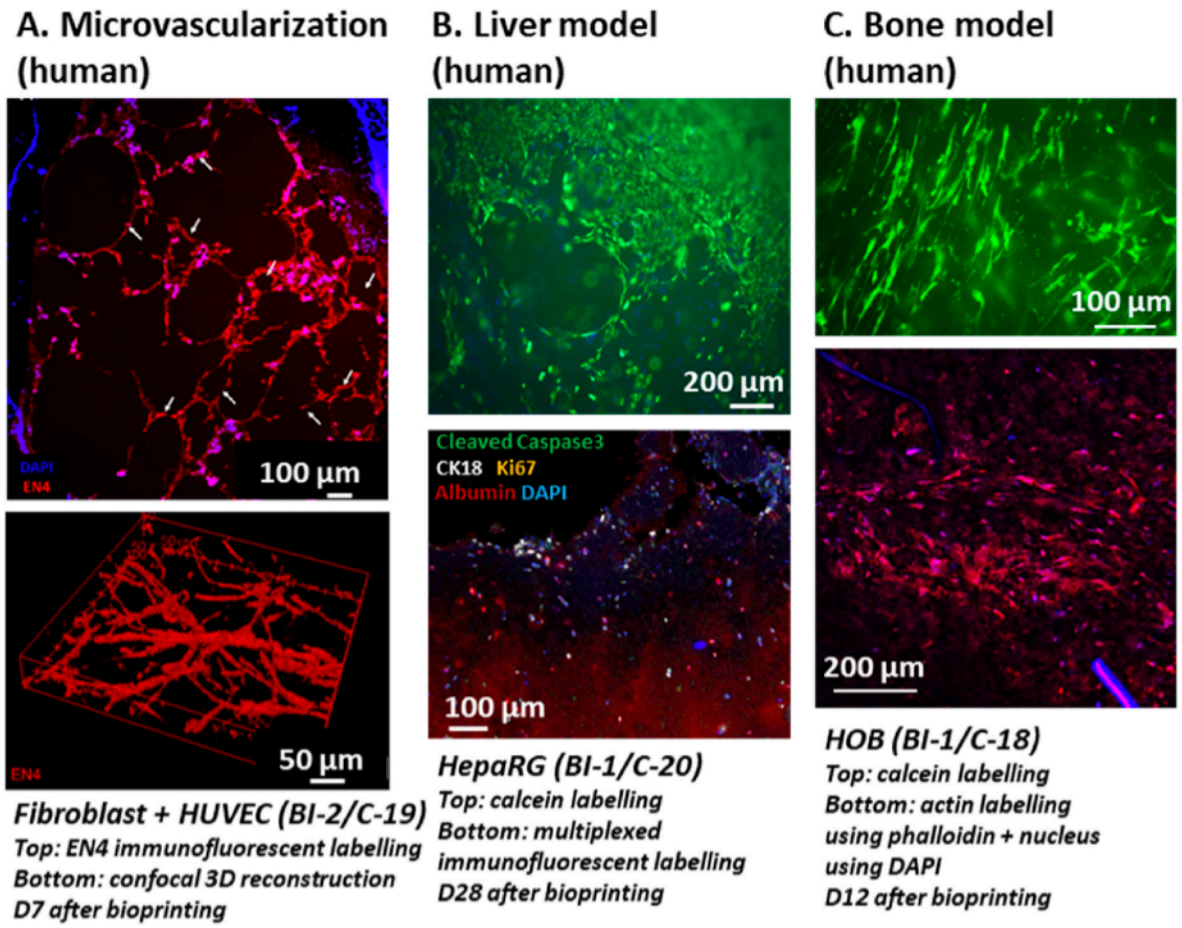

Fig. 5. Human tissues organisation obtained after culture of bioprinted objects (0.3 cm^3: 1 cm*1 cm*3 mm) using the BI-1 formulation of the bio-inspired bioink. A) Microvascularized conjunctive tissue embedding human fibroblast and HUVEC. B) Liver model tissue embedding HepaRG. C) Bone model embedding HOB. Images were obtained after calcein staining or immunohistological labelling.

target tissue. For instance, in breast tissue, an increase in Young's modulus is associated with a higher risk of tumoral transformation [35]. This characteristic has been used to generate healthy and pathological tissues.

Most impressively, 19 different mammalian cell types were successfully bioprinted and cultured using the bio-inspired bioink. This includes all cell types tested by our team and collaborators across the eight labs, demonstrating that so far, no mammalian cells have failed to thrive and develop within or atop the bio-inspired bioink. Furthermore, the majority of these cells exhibited behaviours consistent with their *in vivo* counterparts. Complex microstructures and organizations were readily identified, shedding light on intricate morphogenesis mechanisms resulting in the formation of micro-tubules, micro-vessels, and micro-acini.

It is now evident that microextrusion bioprinting, especially when using bio-inspired bioink formulations, represents a viable avenue for generating a wide range of mammalian soft tissues. We anticipate that numerous future studies will build upon the foundation of the results presented in this work. Our goal of producing large-scale 3D tissues with complex shapes and self-micro-organization is now within reach.

4. Experimental section

4.1. Bioink formulation

3D bioprinting bioinks were formulated using bovine gelatin (Sigma, France), very low viscosity alginate (Alfa Aesar, Thermo Fisher France) and fibrinogen from bovine plasma (Sigma, France). All components were handle under sterile laminar flow to ensure sterility. Stock solution of 0.2 g/mL gelatin, 0.04 g/mL alginate and 0.08 g/mL fibrinogen were dissolved, without any stirring for 18 h at 37 °C, in DMEM (without calcium, with glutamax-1, Invitrogen, France) supplemented with 10 % foetal calf serum (HyClone, USA), 20 µg/ml gentamicin (Pantapharm, France), 100 UI/ml penicillin/streptomycin (Sarbach, France) and 1 µg/ml amphotericin B (Bristol Myers Squibb, France). Table 1 presents the composition of the different formulations used during this study. After 18 h, the bioink components were completely dissolved and homogeneous. The formulations were then prepared by pipetting the component at 37 °C using viscous liquid pipettes, mixed 10-tines by inversion and stored at 37 °C for 15 min for final homogenization.

4.2. Bioink rheological characterisation

A stress-controlled rotational rheometer (DHR2, TA instruments, New Castle, USA) was used to evaluate the rheological behaviour, the viscoelastic balance and the static yield stress value at 21 °C with a 25 mm plate geometry. For rheological behaviour (storage modulus G'), a shear rate sweep was applied to hydrogels from 0.01 to 10 s^{-1}. The viscoelastic balance was evaluated thanks to the phase angle by shear dynamic analysis at frequencies 0.015 Hz, considered to be at rest, and 1.5 Hz, considered to be at flow. Then, the yield stress value was defined by 3iTT test with a shear rate at 30 s^{-1} (mimicking extrusion bioprinting) during 120 s. With this test, the yield stress was calculated with the SAOS-LVER method.

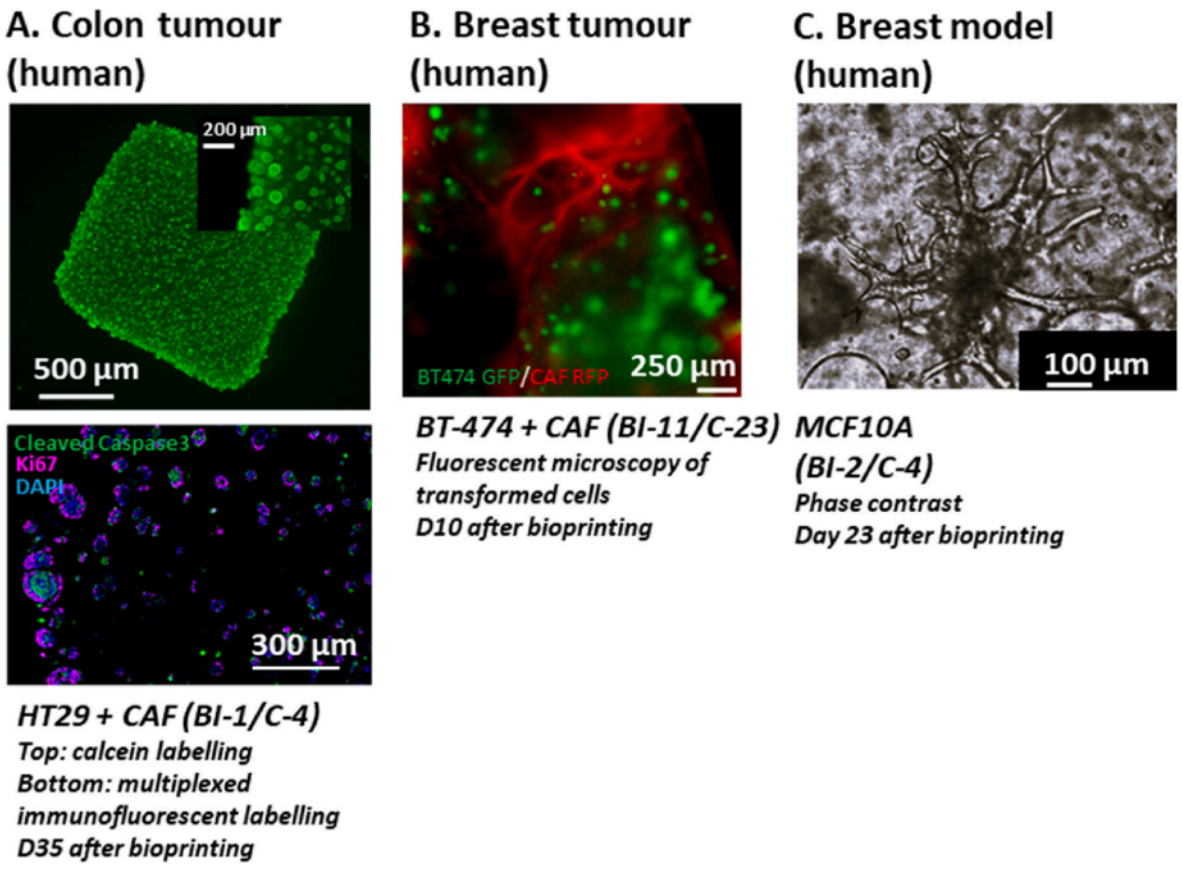

Fig. 6. Human tissues organisation obtained after culture of bioprinted objects (0.3 cm^3: 1 cm*1 cm*3 mm) using the BI-1 formulation of the bio-inspired bioink. A) Colon tumour tissue embedding HT292 and CAF. B) Breast tumour tissue embedding CAF and BT-474. C) Breast model tissue embedding MCF10A. Images were obtained by phase contrast, or after calcein staining or immunohistological labelling.

4.3. 3D bioprinting procedure

Just before printing, each cell type was trypsinized, suspended in fibrinogen to obtain the chosen cells/bioink mL seeding (see Supplementary Table 1) and then formulated with gelatin and alginate to produce the final bioink. After homogenization, a 3 or 10 mL sterile cartridge (Nordson EFD, France) was filled with the bioink, incubated 15 min at 37 °C and then 30 min at room temperature to stabilise the bioink rheological properties. The cartridge was then loaded in a 6-axis robotic bioprinter (BioAssemblyBot®, Advanced Lifescience Solutions, USA) or a BIO X (CELLINK, Sweden) and used to print standardised 0.3 cm^3 bioprinted tissues (1 cm*1 cm*3 mm). A 410 µm diameter, 6.35 mm long needle (Nordson EFD, France) was used to bioprint at a set speed of 10 mm/s.

4.4. Bioprinted tissues consolidation

Bioprinted tissues were consolidated for 90 min at 37 °C in a solution containing at least one of the following components: $CaCl_2$ (Sigma, France), transglutaminase (Ajinomoto Activa WM, Japan) and thrombin (Sigma, France). Table 2 presents the composition of the different consolidation solutions used during the study. Once the consolidation completed, each bioprinted tissue was rinsed three times with sterile NaCl 0.9 % (Versol, France) for 5 min at room temperature.

4.5. Bioprinted tissue culture and monitoring

After the consolidation step, the different bioprinted tissues were grown in non-treated 6- or 12-well plates at 37 °C in a 5 % CO_2 atmosphere, in their dedicated culture medium (Supplementary Table S1). Spent media were recovered in triplicate three times a week and placed at −20 °C until quantification of the lactic acid secreted by cell metabolism.

The lactic acid concentration was quantified using the L-Lactic Acid Assay from Megazyme (L-Lactic Assay Kit, K-LATE, Megazyme, France) for auto-analyzer procedures. The assay was performed according to the manufacturer's instructions. Each sample was deposited in triplicate in the 96-well plate. For highly concentrated samples, dilutions were performed in deionized water and respective commercial fresh medium was used as a negative control. The plates were incubated at 25 °C in the dark for 10 min before measurement of the absorbance at 340 nm with a spectrophotometer (TECAN infinite®).

4.6. DMA measurements

The viscoelastic behaviour of the different consolidated hydrogels was characterised by frequency sweep experiments in DMA in compression mode at 37 °C. These experiments were conducted with a rotational rheometer (DHR2, TA Instruments, Guyancourt, France) with a DMA mode (torque = 0 N) using disk-shaped samples and a parallel plate geometry (8 mm). A preliminary study was performed to define the linear viscoelastic domain, which corresponds to the displacement range where the material properties are assumed to be constant. This domain is determined using oscillatory compression experiments with constant frequency and varying displacement. Then, dynamic compression tests were performed with a frequency range of 0.1–10 Hz (*i.e.* 0.628–62.8 rad/s) at a constant displacement, which is within the linear viscoelastic regime. In these dynamic compression tests, bioprinted tissue undergoes a periodical mechanical strain ε of less than 0.2 %, ε_0 and of angular frequency ω following equation (1):

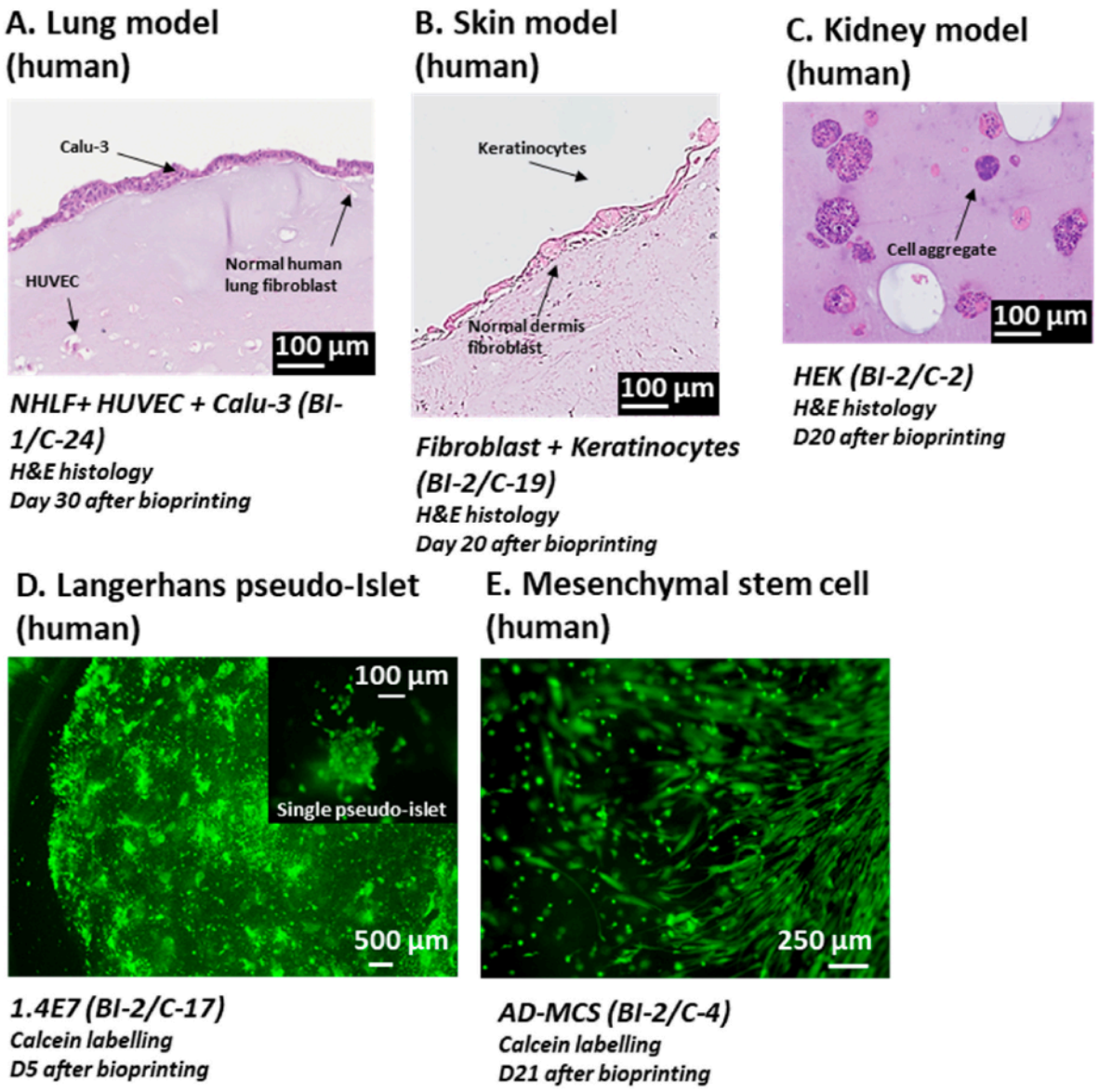

Fig. 7. Human tissues organisation obtained after culture of bioprinted objects (0.3 cm^3: 1 cm*1 cm*3 mm) using the BI-1 formulation of the bio-inspired bioink. A) Lung model tissue embedding NHLF, HUVEC and Calu-3. B) Skin model tissue embedding fibroblast and keratinocytes. C) Kidney model tissue embedding HEK. D) Pancreatic tissue model embedding Langerhans pseudo-islets. E) Mesenchymal stem cell development. Images were obtained after calcein staining, H&E staining or immunohistological labelling.

$$\varepsilon - \varepsilon_0 \; sin \;\; sin\,(\omega t) \qquad \text{Equation (1)}$$

In the case of the generalised Maxwell model, the storage E′(ω) part of the complex modulus is expressed by equation (2):

$$E'(\omega) = E_0\left[1 + \sum_{\alpha=1}^{m} \frac{\beta_\alpha \omega^2 \tau_\alpha^2}{1+\omega^2\tau_\alpha^2}\right] \qquad \text{Equation (2)}$$

$$\eta = E_0 \sum_{\alpha-1}^{m} \beta_\alpha \tau_\alpha \qquad \text{Equation (3)}$$

where E_0 is the Young's modulus of the isolated spring. The relaxation times, τ_α, and the dimensionless reference parameters β_α stand for the contribution of each branch to the global modulus. The overall viscosity η can be defined as equation (3). The time-constant values were regularly distributed between the reciprocals of the highest (62.8 rad/s) and the lowest (0.628 rad/s) angular frequencies of the experimental dynamic modulus. The chosen number of modes was sufficiently high to obtain accurate fitting, but not too large to avoid inconsistent results (*e.g.*, negative values of β_α). This approach led to three-time constants (m = 2), regularly spaced on a logarithmic scale between 5×10^{-2} s and 5×10^{-1} s.

Identification was achieved by solving the following minimization problem described by equation (4):

$$f_{obj}(E_0, \beta_1 \ldots \beta_m) = \sum_{i}^{k} \left[\frac{\left(E_i' - E_i'^{mes}\right)^2}{E_i'^{mes}}\right] \qquad (4)$$

where $E_i'^{mes}$ is the storage modulus obtained from the measured data and E_i' is the one computed with viscoelastic parameters. k is the number of measurements acquired during the frequency sweep compression test. The optimization procedure was performed by using the Microsoft Excel Solver (version 2016) with the Generalised Reduced Gradient (GRG) nonlinear solving method.

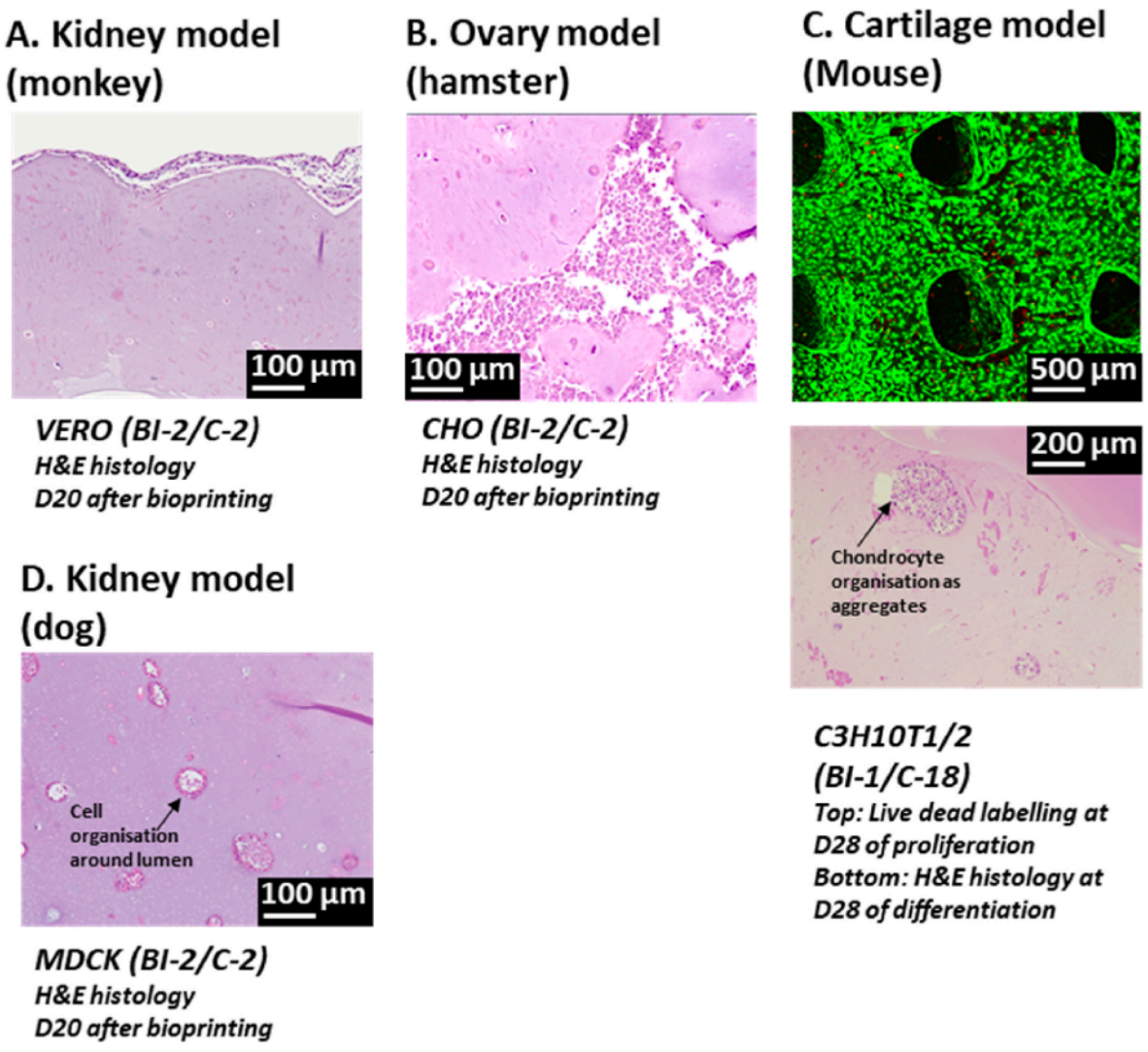

Fig. 8. Animal tissue organisation obtained after culture of bioprinted objects (0.3 cm^3: 1 cm*1 cm*3 mm) using the BI-1 formulation of the bio-inspired bioink. A) Kidney model tissue embedding VERO. B) Ovary model tissue embedding CHO. C) Cartilage model tissue embedding C3H10T1/2. D) Kidney tissue model embedding MDCK. Images were obtained after calcein staining or H&E staining.

Table 1
Final composition of the 10 bioink formulations used in the present study.

CODE	Fibrinogen final g/mL	Alginate very low viscosity final g/mL	Gelatin final g/mL	Gelatin proportion (wt./other components wt.)
BI-1	0.02	0.02	0.05	1.25
BI-2	0.02	0.01	0.1	3.3
BI-3	0.02	0.015	0.075	2
BI-4	0.02	0.005	0.125	5
BI-5	0.02	0.025	0.025	0.56
BI-6	0.02	0.03	0	0
BI-7	0.02	0	0.15	7.5
BI-8	0	0.02	0.05	2.5
BI-9	0	0.01	0.02	2
BI-10	0	0.05	0.1	2

CRediT authorship contribution statement

Christophe A. Marquette: Writing – review & editing, Writing – original draft, Validation, Project administration, Methodology, Investigation, Formal analysis, Data curation, Conceptualization. **Laura Chastagnier:** Investigation. **Benjamin Da Sousa:** Investigation. **Carlos Chocarro-Wrona:** Investigation. **Edwin-Joffrey Courtial:** Data curation. **Elea Rae:** Investigation. **Céline Thomann:** Investigation. **Albane Carre:** Investigation. **Lucie Essayan:** Investigation, Data curation. **Ana J. Pasuch:** Investigation. **Alizée Mosnier:** Investigation. **Chloé Devillard:** Investigation. **Emma Petiot:** Writing – review & editing, Methodology, Investigation, Data curation. **Lucas Lemarié:** Investigation. **Eva-Laure Matera:** Investigation. **Meigge Simoes:** Investigation. **Charles Dumontet:** Conceptualization. **Cristina Cuella Martin:** Investigation. **Léa Pechtimaldjian:** Investigation. **Eve-Isabelle Pécheur:** Investigation. **Véronique Maguer-Satta:** Investigation. **Maude Michelet:** Investigation. **Marie-Laure Plissonnier:** Investigation. **Fabienne Archer:** Investigation. **Karen Moreau:** Investigation. **Marjorie Dufaud:** Investigation. **Cécile Zaupa:** Investigation. **Jean-Marc Balloul:** Investigation. **Quentin Pruvost:** Investigation. **Thibaud Dauphin:** Investigation. **Mathilde Mosser:** Investigation. **Sarah Pragnère:** Investigation.

Declaration of competing interest

The authors declare the following financial interests/personal relationships which may be considered as potential competing interests:

Christophe MARQUETTE reports was provided by University Claude Bernard Lyon 1. If there are other authors, they declare that they have no

Table 2
Final composition of the 24 consolidation solutions used in the present study.

CODE	Ca^{2+} (mM)	Transglutaminase (mg/mL)	Thrombin (U/mL)
C-1	270	40	0
C-2	270	40	10
C-3	27	40	0
C-4	270	4	10
C-5	270	80	0
C-6	270	4.10^{-2}	0
C-7	270	160	0
C-8	270	4.10^{-1}	10
C-9	1360	40	0
C-10	2.7	40	0
C-11	2700	40	0
C-12	0	40	0
C-13	0.27	40	0
C-14	27	40	10
C-15	0	40	0
C-16	270	0	0
C-17	1.8	40	10
C-18	270	2	10
C-19	27	4.10^{-1}	10
C-20	27	4	10
C-21	270	5.10^{1}	10
C-22	0	4.10^{-1}	10
C-23	270	20	10
C-24	2.7	20	10

known competing financial interests or personal relationships that could have appeared to influence the work reported in this paper.

Data availability

Data will be made available on request.

Acknowledgements

All authors contributed equally to this work.
We acknowledge the CIQLE from Université Lyon 1 and the CARTIGEN from CHU Montpellier, for histochemistry, immunohistochemistry and microscopy imaging.

Appendix A. Supplementary data

Supplementary data to this article can be found online at https://doi.org/10.1016/j.bprint.2024.e00351.

References

[1] J.R. Lustig, B.J.G. Strauss, in: B. Caballero (Ed.), Encyclopedia of Food Sciences and Nutrition, second ed., Academic Press, Oxford, 2003.
[2] N.A. Peppas, J.Z. Hilt, A. Khademhosseini, R. Langer, Adv. Mater. 18 (2006) 1345.
[3] M. Zheng, X. Wang, Y. Chen, O. Yue, Z. Bai, B. Cui, H. Jiang, X. Liu, Adv. Healthcare Mater. 12 (2023) 2202042.
[4] A. Tchobanian, H. Van Oosterwyck, P. Fardim, Carbohydr. Polym. 205 (2019) 601.
[5] F. Xu, C. Dawson, M. Lamb, E. Mueller, E. Stefanek, M. Akbari, T. Hoare, Front. Bioeng. Biotechnol. 10 (2022) 849831.
[6] G. Singh, A. Chanda, Biomed. Mater. 16 (2021) 062004.
[7] A. Schwab, R. Levato, M. D'Este, S. Piluso, D. Eglin, J. Malda, Printability and Shape Fidelity of Bioinks in 3D Bioprinting, Chemical Reviews 120 (19) (2020) 11028–11055.
[8] L.J. Pourchet, A. Thepot, M. Albouy, E.J. Courtial, A. Boher, L.J. Blum, C. A. Marquette, Adv. Healthcare Mater. 6 (2017) 1601101.
[9] L. Pourchet, E. Petiot, C. Loubière, E. Olmos, M. Dos Santos, A. Thépot, B.J. Loïc, C. A. Marquette, Bioprinting 13 (2019) e00039.
[10] A. Desanlis, M. Albouy, P. Rousselle, A. Thepot, M. Dos Santos, C. Auxenfans, C. Marquette, J. Tissue Eng. Regen. M 15 (2021) 37.
[11] G. Cidonio, M. Glinka, J.I. Dawson, R.O.C. Oreffo, Biomaterials 209 (2019) 10.
[12] A. Blaeser, D.F. Duarte Campos, U. Puster, W. Richtering, M.M. Stevens, H. Fischer, Adv. Healthcare Mater. 5 (2016) 326.
[13] L. Lemarié, A. Anandan, E. Petiot, C. Marquette, E.-J. Courtial, Bioprinting 21 (2021) e00119.
[14] K. Nair, M. Gandhi, S. Khalil, K.C. Yan, M. Marcolongo, K. Barbee, W. Sun, Biotechnol. J. 4 (2009) 1168.
[15] N. Munir, R.S. Larsen, A. Callanan, Bioprinting 10 (2018) e00033.
[16] B. Webb, B.J. Doyle, Bioprinting 8 (2017) 8.
[17] J. Shi, B. Wu, S. Li, J. Song, B. Song, W.F. Lu, Biomed. Phys. Eng. Exp. 4 (2018) 045028.
[18] a) V.H.M. Mouser, F.P.W. Melchels, J. Visser, W.J.A. Dhert, D. Gawlitta, J. Malda, Biofabrication 8 (2016) 035003;
b) A. Hiller, K. Borchers, G.E.M. Tovar, A. Southan, Addit. Manuf. 18 (2017) 136.
[19] E.J. Courtial, C. Perrinet, A. Colly, D. Mariot, J.M. Frances, R. Fulchiron, C. Marquette, Addit. Manuf. 28 (2019) 50.
[20] a) T. Ikeda, M. Tokita, A. Tsutsumi, K. Hikichi, Jpn. J. Appl. Phys. 28 (1989) 1639;
b) M. Czerner, L.S. Fellay, M.P. Suárez, P.M. Frontini, L.A. Fasce, Proc. Mater. Sci. 8 (2015) 287.
[21] B. Ahvazi, H.C. Kim, S.-H. Kee, Z. Nemes, P.M. Steinert, EMBO J. 21 (2002) 2055.
[22] M. Prokopec, in: P. Dasgupta, R. Hauspie (Eds.), Perspectives in Human Growth, Development and Maturation, Springer Netherlands, Dordrecht, 2001.
[23] L. Ouyang, R. Yao, X. Chen, J. Na, W. Sun, Biofabrication 7 (2015) 015010.
[24] D.A. Herzlinger, T.G. Easton, G.K. Ojakian, J. Cell Biol. 93 (1982) 269.
[25] D.M. Bryant, J. Roignot, A. Datta, A.W. Overeem, M. Kim, W. Yu, X. Peng, D. J. Eastburn, A.J. Ewald, Z. Werb, K.E. Mostov, Dev. Cell 31 (2014) 171.
[26] E.S. Sokol, D.H. Miller, A. Breggia, K.C. Spencer, L.M. Arendt, P.B. Gupta, Breast Cancer Res. 18 (2016) 19.
[27] F.M. Wurm, Processes 1 (2013) 296.
[28] A.S.H. Alchalabi, H. Rahim, E. Aklilu, I.I. Al-Sultan, A.R. Aziz, M.F. Malek, S. H. Ronald, M.A. Khan, Asian Pac. J. Reprod. 5 (2016) 301.
[29] R. Parent, M.J. Marion, L. Furio, C. Trépo, M.A. Petit, Gastroenterology 126 (2004) 1147.
[30] M. Nie, B. Kong, G. Chen, Y. Xie, Y. Zhao, L. Sun, Bioact. Mater. 17 (2022) 369.
[31] I.K. Moutsatsos, G. Turgeman, S. Zhou, B.G. Kurkalli, G. Pelled, L. Tzur, P. Kelley, N. Stumm, S. Mi, R. Müller, Y. Zilberman, D. Gazit, Mol. Ther. 3 (2001) 449.
[32] M. Oliver-Ferrándiz, L. Milián, M. Sancho-Tello, J.J. Martín de Llano, F. Gisbert Roca, C. Martínez-Ramos, C. Carda, M. Mata, Biomedicines 9 (2021).
[33] J.T. McCluskey, M. Hamid, H. Guo-Parke, N.H. McClenaghan, R. Gomis, P.R. Flatt, J. Biol. Chem. 286 (2011) 21982.
[34] H. Guo-Parke, J.T. McCluskey, C. Kelly, M. Hamid, N.H. McClenaghan, P.R. Flatt, J. Endocrinol. 214 (2012) 257.
[35] A.J. Ironside, J.L. Jones, Oncotarget 7 (2016) 31550.